Resource

Cell

Functional Genomic Landscape of Human Breast Cancer Drivers, Vulnerabilities, and Resistance

Graphical Abstract

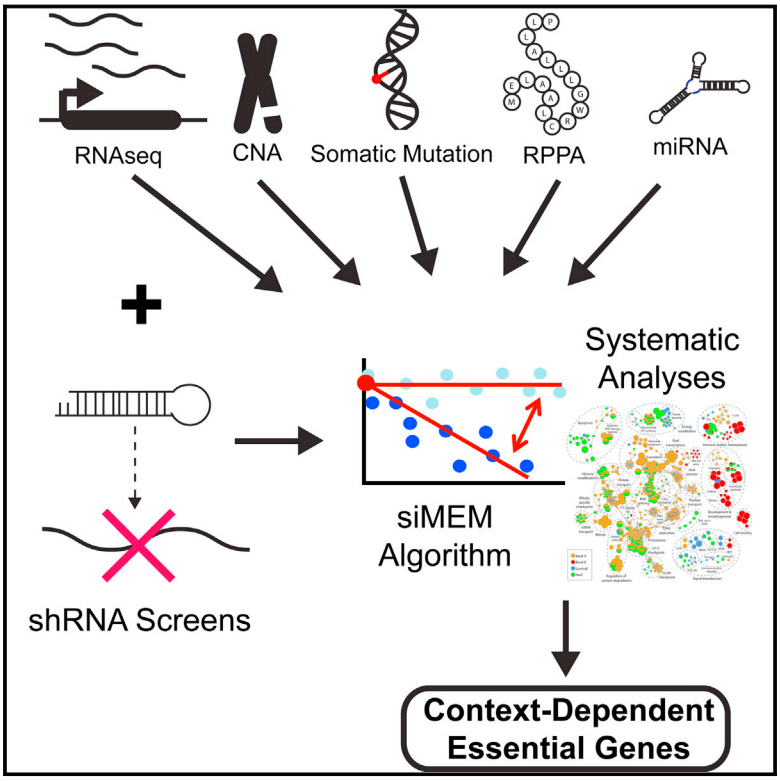

Authors

Richard Marcotte, Azin Sayad, Kevin R. Brown, ..., Dana Pe'er, Jason Moffat, Benjamin G. Neel

Correspondence

benjamin.neel@nyumc.org

In Brief

Pooled shRNA screens of a large panel of breast cancer cell lines, coupled with an improved analytical tool, siMEM, and integration with genomic and proteomic data, identify general and context-dependent essential genes in breast cancer. This study constitutes the largest functional characterization of breast cancer to date.

Highlights

- We screened 77 breast cancer lines using a genome-wide pooled shRNA library
- We developed an algorithm (siMEM) to improve identification of context-dependent genes
- Integrating screen results with genomic data reveals potential "drivers"
- *BRD4* is essential for luminal cancer, and mutant *PIK3CA* confers BET-I resistance

Accession Numbers

GSE73526
GSE74702

Marcotte et al., 2016, Cell *164*, 293–309
January 14, 2016
http://dx.doi.org/10.1016/j.cell.2015.11.062

CellPress

Resource

Cell

Functional Genomic Landscape of Human Breast Cancer Drivers, Vulnerabilities, and Resistance

Richard Marcotte,[1,9,12] Azin Sayad,[1,9] Kevin R. Brown,[2] Felix Sanchez-Garcia,[4] Jüri Reimand,[2,10] Maliha Haider,[1] Carl Virtanen,[1] James E. Bradner,[5,6] Gary D. Bader,[2] Gordon B. Mills,[7] Dana Pe'er,[4] Jason Moffat,[2,3] and Benjamin G. Neel[1,8,11,*]

[1]Princess Margaret Cancer Centre, University Health Network, Toronto, ON M5G 1L7, Canada
[2]The Donnelly Centre
[3]Department of Molecular Genetics
University of Toronto, ON M5S 3E1, Canada
[4]Columbia University, New York, NY 10027, USA
[5]Department of Medical Oncology, Dana-Farber Cancer Institute
[6]Department of Medicine
Harvard Medical School, Boston, MA 02215, USA
[7]Department of Systems Biology, Sheikh Khalifa Al Nahyan Ben Zayed Institute for Personalized Cancer Therapy, University of Texas MD Anderson Cancer Center, Houston, TX 77030, USA
[8]Laura and Isaac Perlmutter Cancer Centre, NYU-Langone Medical Center, NY 10016, USA
[9]Co-first author
[10]Present address: Ontario Institute for Cancer Research, Toronto, ON M5G 0A3, Canada
[11]Present address: Laura and Isaac Perlmutter Cancer Centre, NYU-Langone Medical Center, NY 10016, USA
[12]Present address: National Research Council, Royalmount Avenue, Montreal, QC H4P 2R2, Canada
*Correspondence: benjamin.neel@nyumc.org
http://dx.doi.org/10.1016/j.cell.2015.11.062

SUMMARY

Large-scale genomic studies have identified multiple somatic aberrations in breast cancer, including copy number alterations and point mutations. Still, identifying causal variants and emergent vulnerabilities that arise as a consequence of genetic alterations remain major challenges. We performed whole-genome small hairpin RNA (shRNA) "dropout screens" on 77 breast cancer cell lines. Using a hierarchical linear regression algorithm to score our screen results and integrate them with accompanying detailed genetic and proteomic information, we identify vulnerabilities in breast cancer, including candidate "drivers," and reveal general functional genomic properties of cancer cells. Comparisons of gene essentiality with drug sensitivity data suggest potential resistance mechanisms, effects of existing anti-cancer drugs, and opportunities for combination therapy. Finally, we demonstrate the utility of this large dataset by identifying BRD4 as a potential target in luminal breast cancer and *PIK3CA* mutations as a resistance determinant for BET-inhibitors.

INTRODUCTION

Breast cancer is the second leading cause of cancer death in women. Better detection and therapy have led to >85% 5-year survival, yet half of affected women die from their disease. This outcome reflects incomplete understanding of the molecular alterations, heterogeneity, and determinants of drug response in breast tumors. Genetic and epigenetic abnormalities in breast cancer have been defined, but identifying causal defects and exploiting them for target discovery remain challenging.

"Breast cancer" actually comprises molecular subtypes that predict prognosis and drug response. Early profiling studies identified "intrinsic subtypes": luminal A and B, basal-like (basal), HER2$^+$ and normal-like (Perou et al., 2000; Sørlie et al., 2001). These were joined by a "claudin-low" subtype that, like basal breast cancer, is typically estrogen receptor-negative (ER$^-$), progesterone receptor-negative (PR$^-$), and HER2-negative (HER2$^-$) (Hennessy et al., 2009; Prat et al., 2010). Basal and luminal B tumors have the worst prognosis; claudin-low tumors have intermediate outcome (Prat et al., 2010). Clinically, intrinsic subtypes can be defined by the "PAM50" classifier (Parker et al., 2009).

These molecular subtypes complement, but do not fully overlap, pathologic classification by ER, PR, and HER2 status (Parker et al., 2009). Luminal tumors are typically ER$^+$/PR$^+$, and basal tumors are usually "triple negative" (ER$^-$, PR$^-$, HER2$^-$). Breast cancer cell lines generally fall into four subtypes: basal A or B, HER2$^+$, and luminal (Neve et al., 2006; Prat et al., 2010). Basal A lines resemble "basal" tumors; basal B lines are enriched for claudin-low genes.

Recent large-scale RNA and proteomic profiling studies have further divided luminal and "triple negative" breast cancer (TNBC) into at least ten subtypes (Curtis et al., 2012; Lehmann et al., 2011; Cancer Genome Atlas Network, 2012), and next-generation sequencing (NGS) has identified multiple aberrations in breast tumors (Banerji et al., 2012; Ellis et al., 2012; Shah et al.,

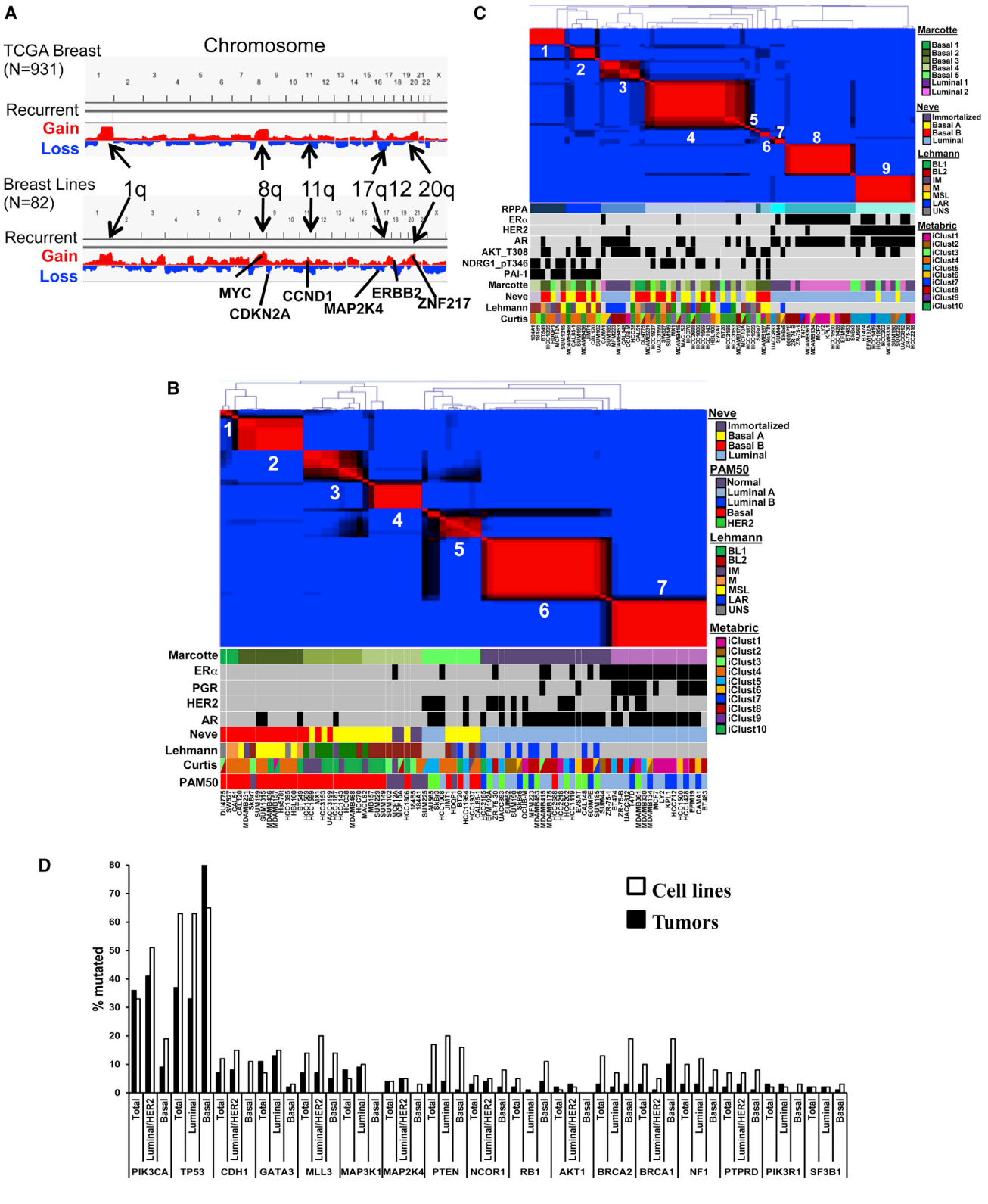

(legend on next page)

2012; Stephens et al., 2012; Cancer Genome Atlas Network, 2012). Whether breast cancer lines represent these new categories and have mutational profiles like tumors remains unresolved.

Moreover, genomics often cannot distinguish "passenger" mutations from "drivers" that promote tumorigenesis and might be therapeutic targets. Highly recurrent defects (e.g., HER2 amplification) point to drivers and some have led to "targeted therapies" (e.g., Trastuzumab). Many other abnormalities, some clearly oncogenic, occur at low frequency, and some drivers are difficult to target (e.g., *MYC*, *RAS*). However, the collateral genotoxic, proteotoxic, and metabolic stresses caused by the abnormal tumor genome can cause "emergent dependencies," potentially providing alternate therapeutic options.

Functional genomics, partnered with genomic data, can identify targets coupled to biomarkers (Zender et al., 2008). Pooled shRNA libraries enable genome-wide "drop-out" screens, which can identify cancer drivers and context-dependent events. Several groups have performed shRNA screens (Cheung et al., 2011; Marcotte et al., 2012), but most surveyed relatively few cell lines of the same cancer type and none represented the diversity of neoplasms such as breast cancer. Here, we report the results of genome-wide shRNA screens of >75 breast cancer lines with genomic, transcriptomic, and proteomic annotation. Employing an improved statistical framework (siMEM), we provide an integrated map of subtype- and context-dependent essentiality in breast cancer cells.

RESULTS

Breast Cancer Lines Are Reasonable Models

We performed genomic and proteomic analysis on 78 breast cancer and four immortalized mammary cell lines (Table S1A). Copy number abnormalities (CNAs) were similar ($r = 0.7$) in lines and breast tumors, with all major CNAs represented (Figures 1A and S1A). RNA sequencing (RNA-seq) and non-negative matrix factorization (NMF) yielded seven clusters (Figures 1B and S1B). Compared with the Neve classification (Neve et al., 2006), we found four basal, two luminal/HER2$^-$, and one mixed cluster(s). The extra basal clusters mainly sub-divided the basal A and B subtypes (Figures 1B and S1C) and resembled the additional subgroups seen in an extensive survey of TNBC (Lehmann et al., 2011). Most luminal/HER2 cell lines fell into Clusters 6 and 7, which were distinguished by *ERBB2* and *ESR1* expression, respectively. The NMF clusters also related to specific METABRIC "iClusters" (Curtis et al., 2012). Every iCluster was present in the panel, although iClusters 2 and 7 each were represented by less than five lines (Figure S1C). Lines defined as "basal" by PAM50 generally fell into our basal clusters and those of Lehmann (Lehmann et al., 2011), but PAM50-derived signatures did not place luminal/HER2 lines into subgroups similar to those seen by NMF or the Curtis classification.

The top 50% variable proteins by reverse-phase protein array (RPPA) formed nine clusters by NMF (Figures 1C and S1D). With few exceptions, RPPA-(R) and RNA clusters differed markedly. Most (13/18) HER2$^+$ lines fell into R-Cluster 9. R-Cluster 8 consisted mainly of expression-derived Cluster 7 lines and was driven by ERα, GATA3, and BCL2. Two small R-clusters were enriched for luminal/HER2 lines: R-Cluster 3 was mainly ER$^-$/AR$^+$ and featured high p-AKT (pT308 and pS473) and p-AMPKα (pT172). R-Cluster 7 (three lines) was distinguished by high G6PD, p-4EBP, and reactivity to a VHL antibody that cross-reacts with Epiplakin. The other R-clusters were enriched for basal lines. R-Cluster-1 contained three of the four "normal breast" lines and was driven by NDRG1, MYC, TAZ, and p-YAP. R-Cluster 2 also had high NDRG1, MYC, TAZ, and p-YAP, as well as high PAI-1 and phospho- and total EGFR (Table S1B). R-Cluster-4, the largest, was a default basal cluster.

Exome sequencing of genes mutated in ≥3% of breast tumors in COSMIC and TCGA (Table S1C) showed that all frequent somatic mutations in breast cancer were found in our cell line panel. *TP53* and *PIK3CA* mutations (23% and 26%, respectively, in tumors) were seen in 63% and 33% of lines, respectively. *TP53* is mutated more often in TNBC/basal tumors (80% versus 26%) (Cancer Genome Atlas Network, 2012), but its mutation frequency was similar in basal and luminal/HER2 lines. For most genes, mutation rate and distribution were comparable in tumors and lines (Figure 1D).

We also profiled microRNAs (miRNAs) by NanoString. ERα is the major determinant of miRNA levels in breast tumors (Dvinge et al., 2013; Riaz et al., 2013). Similarly, unsupervised clustering revealed three miRNA groups in cell lines, two basal and one luminal (Figure S1E). Overall, we conclude that a sufficiently large cell line panel represents the genomic and proteomic landscape of breast tumors and provides a reasonable template for identifying context-dependent essential genes.

Improved Prediction of Gene Essentiality

To identify genes required for proliferation/survival ("essentials"), we used pooled lentiviral shRNA dropout screens (Marcotte et al., 2012). Nearly all (77/82) lines gave satisfactory data (Table S1A). Using our earlier metric, zGARP, we scored 402 genes as essential in at least 50% of lines (Table S2A). These included most (261/297 and 218/291, respectively) genes defined earlier as "general essential" or "core essential" in ovarian, pancreas, and selected breast cancer lines (Hart et al., 2014; Marcotte et al., 2012). Not surprisingly, genes annotated as having "housekeeping" roles (e.g., translation, splicing, proteasome, cell cycle) were prominent general essentials (Table S2B).

Figure 1. Genomic/Proteomic Characterization

(A) CNA profiles of breast tumors (top) from TCGA and cell lines (bottom).

(B) NMF clustering of RNA-seq data for breast cancer lines. *ESR1* (ER), *ERBB2* (HER2), *PGR* (PR), and *AR* (AR) expression are represented by black squares. Lines were assigned to published subtypes (colored boxes).

(C) NMF clustering of RPPA data.

(D) Frequency of indicated mutations in cell lines and tumors, grouped into basal and luminal/HER2 subtypes. Tumor data are from COSMIC.

See also Figure S1 and Table S1.

A

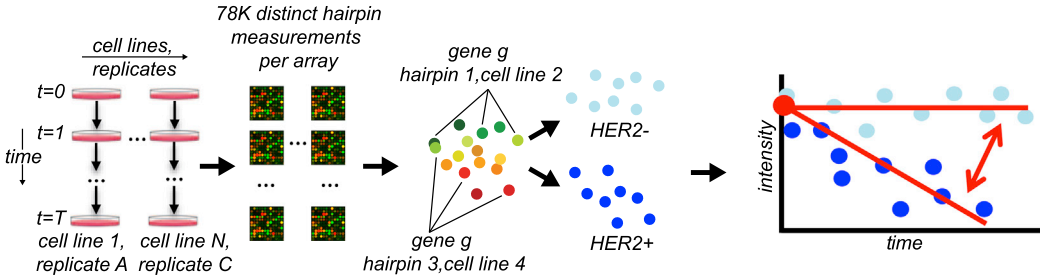

B

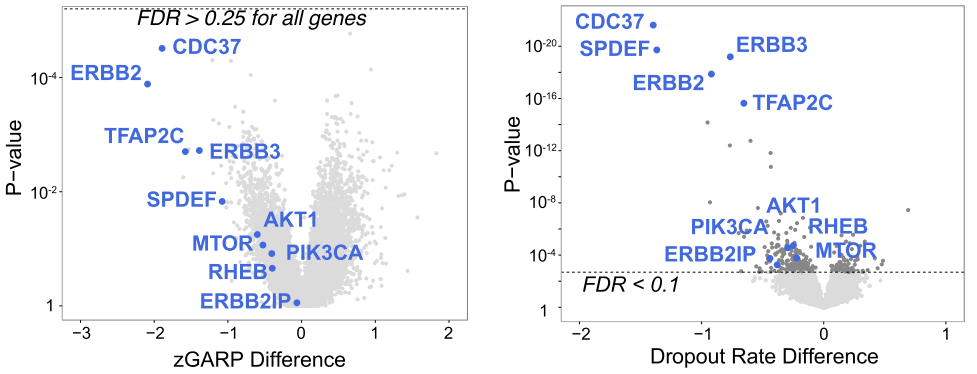

C

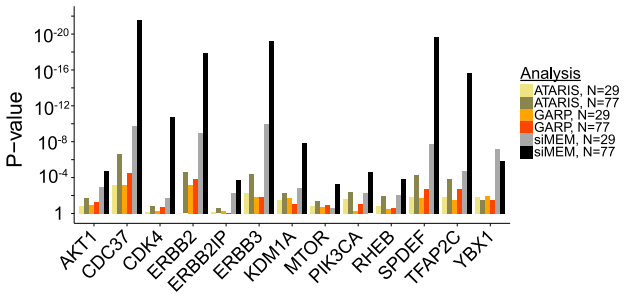

D

Achilles dataset (N=102)		ATARIS			siMEM		
analysis	gene	p-value	FDR	rank	p-value	FDR	rank
BRAF mutant vs. normal	*BRAF*	$2x10^{-5}$	0.143	1	$3x10^{-14}$	$3.1x10^{-10}$	1
KRAS mutant vs. normal	*KRAS*	$2x10^{-5}$	0.157	1	$7.3x10^{-8}$	$2x10^{-4}$	1
	BCL2L1	Not Significant			$1.4x10^{-5}$	0.025	6
PIK3CA mutant vs. normal	*PIK3CA*	$2x10^{-5}$	0.053	1	$5x10^{-9}$	$5.1x10^{-5}$	3
More essential with increasing expression (N=83 samples with matching CCLE expression)	*HNF1B*	$2x10^{-5}$	0.075	1	$3.2x10^{-9}$	$2.2x10^{-6}$	3
	PAX8	$2x10^{-5}$	0.075	2	$2.93x10^{-6}$	$6.97x10^{-4}$	6
	E2F3	$4x10^{-5}$	0.075	3	$8.01x10^{-5}$	0.01	11
	SOX10	$6x10^{-5}$	0.075	5	$1.81x10^{-11}$	$2.29x10^{-8}$	1
	BCL2L1	$1.4x10^{-4}$	0.096	9	$1.72x10^{-10}$	$1.74x10^{-7}$	2
	MYB	$3.4x10^{-4}$	0.213	12	0.003	0.111	70
	KRAS	Not Significant			$7.16x10^{-8}$	$3.62x10^{-5}$	4
	HDAC4	Not Significant			$1.4x10^{-4}$	0.016	13
	MAP3K3	Not Significant			$5.2x10^{-4}$	0.037	23
	MYC	Not Significant			$7.2x10^{-4}$	0.047	24
	CCNE1	Not Significant			$8.7x10^{-4}$	0.052	31
	JAK3	Not Significant			$9.4x10^{-4}$	0.054	32

(legend on next page)

By contrast, neither zGARP, nor other algorithms (ATARIS [Shao et al., 2013], RIGER [Barbie et al., 2009], RSA [König et al., 2007]), identified known subtype-specific essential genes from our large dataset. Such methods summarize replicate shRNA measurements into single "hairpin" or "gene" scores, which are compared between subtypes by t tests or similar statistics. This approach leads to loss of information about measurement variance, limiting statistical power to detect biological differences.

Hierarchical ("mixed-effect") linear models allow systematic measurement effects, such as hairpin differences or heterogeneous genetic contexts, to be specified and used in significance calculations. Such a model could increase sensitivity for detecting biological differences in screens by avoiding information loss, while limiting false positives. We therefore developed the small interfering RNA (siRNA)/shRNA mixed-effect model (siMEM), which considers the level of each shRNA to be a regression function of its initial abundance, baseline trend in abundance over time, and difference in abundance trend between samples sharing a common feature (Figures 2A, S2A, and S2B; Supplemental Experimental Procedures).

Using siMEM and previous metrics, we sought genes selectively required in HER2$^+$ lines (n = 17). Reassuringly, siMEM-detected known HER2$^+$-associated essentials ("known positives"), such as *ERBB2*, its dimerization partner *ERBB3*, PI3K/mTOR pathway members (*PIK3CA*, *AKT1/2*, *RHEB*, *MTOR*), *CDC37* (encodes an ERBB2 co-chaperone), and two transcription factors (*TFAP2C*, *YBX1)* in the HER2 (ERBB2) pathway. Almost none of these survived false discovery rate (FDR) correction using GARP or ATARIS (Figure 2B; Table S2C). Only siMEM predicted "known positives" from the data in our earlier screen (Marcotte et al., 2012) and it greatly improved their prediction rankings and p values (Figures 2C and S2C). When classes (normal/HER2$^+$) were shuffled randomly for each gene, siMEM p values were close to the expected uniform distribution (Figure S2D). Regression structures that ignored systematic measurement effects produced many (incorrectly) significant p values (Figures S2E and S2F). By contrast, siMEM produced the best fit and ranking of known positives (Figures S2B, S2G, and S2H). Finally, we applied siMEM and ATARIS to the "Achilles" dataset (Cheung et al., 2011): siMEM was better at predicting *BRAF*, *KRAS*, or *PIK3CA* essentiality in cognate mutant cells and in finding genes more essential with increased expression, which are enriched for drivers (Figure 2D; also see below).

Breast- and Subtype-Specific Essential Genes

We focus here on gene essentiality relative to the Neve classification, which most closely resembles clinical subtypes, but Tables S3A–S3G provide essentiality data for each subtype in Figures 1B and 1C. Comparing basal with luminal/HER2 cell lines, we found 975 and 985 subtype-specific essentials (FDR < 0.1), respectively (Figure 3A; Tables S3F and S3G). The top luminal/HER2-essentials were *FOXA1*, a pioneer factor for ERα (Lupien et al., 2008), *SPDEF*, which promotes luminal differentiation and survival of ERα$^+$ cells (Buchwalter et al., 2013), *CDK4* and *CCND1*, which form a complex targeted by Palbociclib in ER$^+$ breast cancer (Dhillon, 2015), and *TFAP2C*, which directs *ERBB2* expression (Bosher et al., 1995). Other "expected" luminal/HER2-essential genes included PI3K/mTOR pathway components *(PIK3CA*, *PDPK1*, *AKT1/2*, *RHEB*, *MTOR*) and ER-interacting proteins/co-activators (*KMT2D*, *EP300*, *GATA3*, *KDM1A*, *DNM1L*, *NCOA2*).

The top basal-selective essentials, *PSMB3* and *PSMA6*, encode proteasome subunits (Table S3F), a dependency seen earlier (Petrocca et al., 2013). The next most essential basal-specific gene was *ATP6V1B2*, which encodes a component of the vacuolar ATPase required for lysosomal acidification that is the target of Bafilomycin A1 (BafA1). Notably, basal lines were 5-fold more sensitive and basal A lines were 7-fold more sensitive to BafA1 than luminal/HER2 lines (Figures S3A and S3B). Other genes reputedly more important in basal breast cancer scored as "basal-essential," including *PLK1*, *EGFR*, *FZD7*, *SLC7A11*, *CTNNB1*, *LRP5*, *FZD8*, and *TWIST2* (Jamdade et al., 2015; Maire et al., 2013; Timmerman et al., 2013), but we also saw other potential vulnerabilities (Table S3F).

We selected several subtype-specific genes for orthogonal testing with siRNAs. Multiple basal-specific, luminal-specific, and HER2-specific genes validated and demonstrated the predicted subtype preference (Figure 3B; Table S3L). Overall, the validation rate was ~70%, with most siRNAs showing >80% knockdown (Figure 3C; data not shown).

The genomics of basal breast cancer and high-grade serous ovarian cancer (HGSC) are very similar (Cancer Genome Atlas Research Network, 2011; Cancer Genome Atlas Network, 2012). Remarkably, in a pairwise comparison with luminal-specific (this screen) or HGSC- or pancreatic cancer-specific essentials (Marcotte et al., 2012), only 20 essential genes differed between basal breast cancer and HGSC. By contrast, thousands of differences were seen in all other comparisons (Figure S3C).

We analyzed subtype-specific essential gene sets for preferred pathways and protein-protein interactions (PPIs) (Figures 3D and 3E; Tables S3H–S3K). As expected, HER2-specific essential pathways included EGF, PI3K, and mTOR signaling. Other functions important in this subtype included regulation of eIF2, aerobic ATP synthesis/TCA cycle, chromatin-modifying enzymes, "response to gamma radiation" (including *YAP1*, *ATR*, and *ATM*), as well as an EP300/BRCA1 PPI sub-network (Table S3J). EP300 is a BRCA1 co-activator (Pao et al., 2000), and BRCA1 is phosphorylated via the PI3K/AKT pathway, which also is required in HER2$^+$ lines (Figure 2C; Tables S2C and S3B).

Figure 2. siMEM Overview

(A) Experimental scheme. Samples were hybridized to microarrays and dropout was quantified. Hierarchical linear regression summarizes data as a combination of initial measurement intensity, baseline trend, and difference in essentiality associated with changes in a genomic covariate (light blue versus dark blue).

(B) Volcano plot of zGARP (left) and siMEM (right) essentiality differences associated with HER2$^+$ lines. Dotted lines show FDR cut-off.

(C) siMEM produces the best p values for known positives.

(D) *BRAF*, *PIK3CA*, or *KRAS* mutant versus normal and expression versus essentiality analyses of the Achilles dataset (n = 102).

See also Figure S2, Table S2, and Supplemental Experimental Procedures.

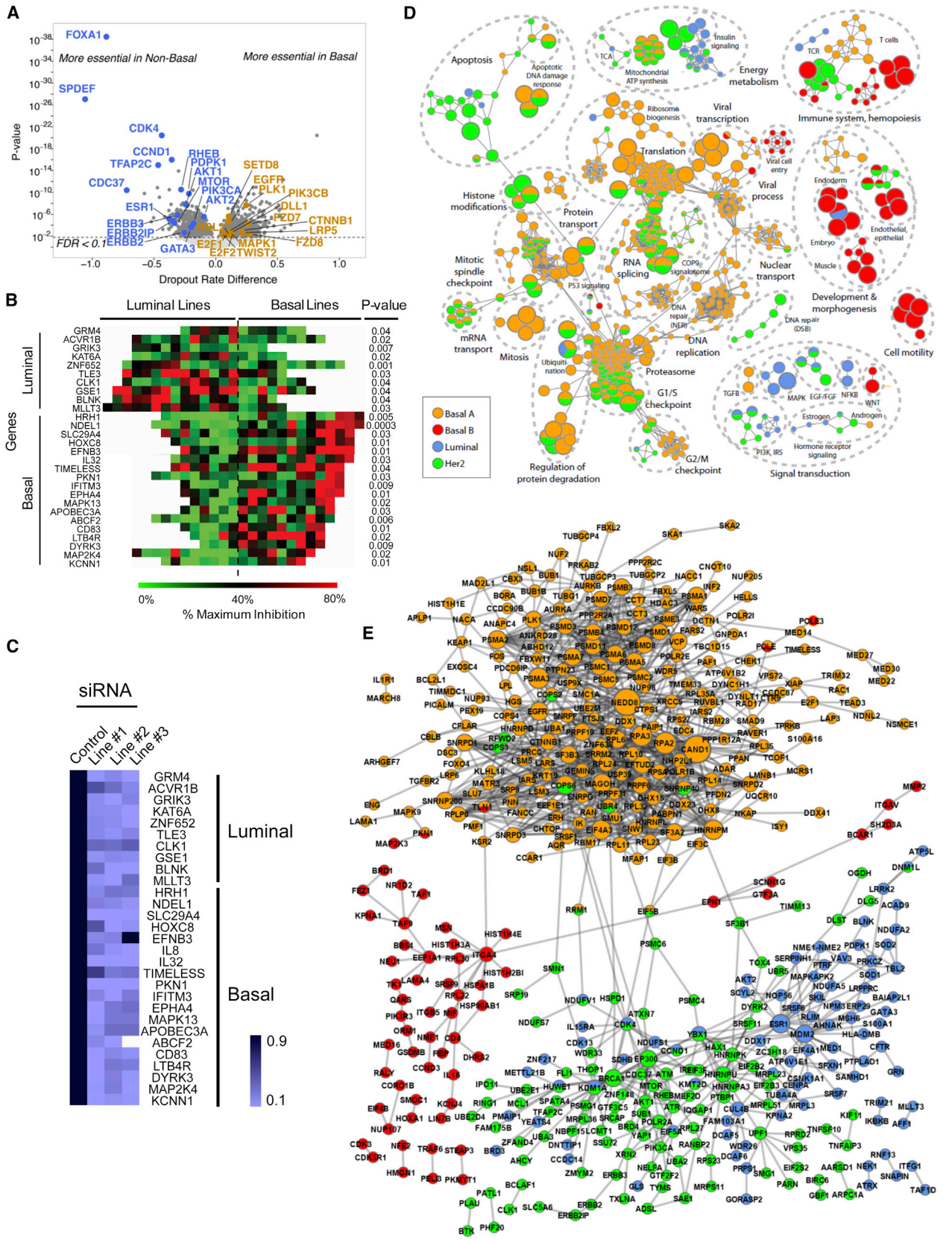

(legend on next page)

Notably, ATM is essential for HER2$^+$ tumors (Stagni et al., 2015) and it also phosphorylates BRCA1 (Cortez et al., 1999; Gatei et al., 2000). Preferential sensitivity to loss of DNA damage sensors might explain the observed synergy of chemotherapy and Trastuzumab.

Top enriched pathways and PPIs for basal A lines were dominated by genes for splicing, the proteasome and mitosis (Figures 3D and 3E; Table S3H). Other required functions included the COP9 signalosome (CSN) and a PPI sub-network defined by CAND1/NEDD8 (Figure 3E). CSN and CAND1/NEDD8 regulate SKP1/CUL1/F-box (SCF) complexes (Flick and Kaiser, 2013). While the core SKP1/CUL1 complex showed no subtype specificity, several F-box genes were selectively essential in basal A lines, including *FBXW11*/β-*TrCP2* (Table S3B). *FBXL6* and *FBXO15* were more essential in basal B or luminal/HER2 lines, respectively (Table S3B; data not shown). Hence, F-box proteins might impart subtype-specific functions to SKP1/CUL1.

Lack of functional annotation (<50% of genes annotated) resulted in a relative paucity of basal B and luminal nodes when compared to basal A- and HER2- nodes (>65% of genes annotated, Figures S3D–S3F). Nevertheless, essential pathways and PPI networks for luminal lines included epithelial development, MDM2, PI3K, and hormone receptor (*ESR1*) signaling (Figures 3D and 3E). The latter two are targets of known drugs for luminal breast cancer. Less expected "luminal-enriched" pathways/PPIs included redox-related (SOD1, SOD2, ENOX1) and mitochondrial (e.g., electron transport chain, mitochondrial ribosome) proteins. By contrast, basal B-essentials were enriched for genes related to polarity (*PARD3*, *PAR3D*), cell-cell junctions and adhesion (*CDH2*, *CLDN1*, *CLDN4*, *ITGA4*, *ITGAV*, *ITGB5*), embryonic development, organ morphogenesis, fatty acid metabolism, and T cell immunity (Figures 3D and 3E). Some of these genes, such as *SOX9* (Guo et al., 2012a), *KLF4* (Yu et al., 2011), and *ALOX5AP* (Kim et al., 2005), have reported roles in breast cancer, although not specifically in basal B tumors.

cis- and *trans*-Essential Interactions with Common CNAs

There are hundreds of CNAs in breast cancer (Curtis et al., 2012; Cancer Genome Atlas Network, 2012), yet for most, the key driver gene(s) is unclear. METABRIC defines 30 regions of copy number gain and 15 deletions (Curtis et al., 2012). ISAR, being more sensitive for small amplicons, identifies 83 recurrent CNAs (Sanchez-Garcia et al., 2014). We predicted significant (FDR < 0.2) *cis*-essential genes (more essential in amplicon$^+$ lines) for 9/83 ISAR regions. Four corresponded to genes in a METABRIC amplicon (Figure S4A; Table S4A): *EGFR* (ISAR(I)-34/METABRIC(M)-10), *CCND1* (I-52/M-21), *ERBB2* (I-70/M-35), and *TFAP2C* (I-81/M-42). The others were unique to ISAR-defined regions (Table S4B): *CTSS* (I-6), *ESR1* (I-30), *RALGAPA1* (I-62), *FOXA1* (I-63), and *BCL2* (I-76).

Even for known drivers (or for deletions), targeting the key gene can be difficult. "*trans*-Essential" genes can suggest alternative strategies. Combining all METABRIC regions, we identified 2,560 *trans*-essentials, an average of 58 per CNA (range 0–285; Figures 4A and S4A; Table S4A). Only 61 (∼3%) *trans*-essentials showed significantly increased or decreased expression in sensitive lines (Figure S4B and Supplemental Experimental Procedures); hence, most would not be found by gene expression surveys. Expected *trans*-essentials were seen for the *CCND1* (*CDK4*, *USP18*) (Guo et al., 2012b) and *ERBB2* (*ERBB3*, *CDC37*, *PIK3CA*) amplicons and for *CDKN2A* deletions (*CCND1*, *CDK6*) (Figures 2B and S4A; Table S4A). It can be difficult to know if a *trans*-essential is "expected" for deletions, especially if the cognate tumor suppressor is undefined. Even so, we saw intriguing associations with "druggable" targets for region 27, containing *RB1* (more sensitive to *MAP2K2* depletion), region 11 (more sensitive to *TLK2*, *BRD4*, or *ACVR1B* depletion), and region 40 (more sensitive to *PTK6* or *MAP2K4* depletion) (Table S4A).

METABRIC region 14 includes *MYC*, which is generally deemed "undruggable." Notably, *MYC* was the most essential gene in region 14-amplified lines (Figure 4A), but was not differentially essential by FDR, probably because of its requirement in most tumor cells (Dang, 2012). Pathway analysis of the 91 region 14 *trans*-essentials (FDR < 0.2; Table S4A) revealed genes for mitosis, DNA replication, and RNA metabolism (Table S4C), all known MYC functions (Dang 2012). MYC transcriptional targets (Figure 4B) and genes encoding MYC-interacting proteins (Table S4D) also were strongly enriched: 46% of *MYC trans*-essential genes were MYC transcriptional targets/interactors. We tested two *MYC trans*-essentials potentially amenable to drug discovery; indeed, amplified lines were preferentially sensitive to *MINK1* or *USP5* depletion (Figure 4C). We also validated *YAP1* and *BRCA1* as *trans*-essential for METABRIC regions 35 (contains *ERBB2*), and 36 (putative driver: *ZNF652*), respectively (Figures S4C and S4D).

HELIOS integrates CNA, expression, mutation, and essentiality into a single score that predicts *cis*-essential genes (Sanchez-Garcia et al., 2014). The initial HELIOS report, using data from our earlier screen, identified and validated ten potential drivers. Using our expanded dataset, the HELIOS score increased for most known drivers and previously validated genes (Figure 4D; Table S4E). We also tested two new predictions and found that amplicon$^+$ lines were more sensitive to siRNA-mediated depletion (Figure 4E).

Figure 3. Subtype-Specific Essential Genes

(A) Volcano plot of basal-specific and luminal/HER2-specific essentials.

(B) Heatmap shows % proliferation-inhibition, compared to general essential *RPL9* (100% inhibition), after pooled siRNA treatment (p values: one-sided t test).

(C) Knockdown efficiency (by qRT-PCR) of siRNAs for genes in (B).

(D) Subtype-specific pathways. Each node represents a process; functionally similar nodes are grouped and labeled by enriched function. Nodes are colored according to the subtype in which the process is enriched; processes enriched in more than one subtype have multiple colors. Red, basal B; orange, basal A; green, HER2$^+$; blue, luminal.

(E) PPI networks for subtype-specific genes. Nodes represent genes and are multi-colored if present in multiple subtypes; edges represent interactions.

See also Figure S3 and Table S3.

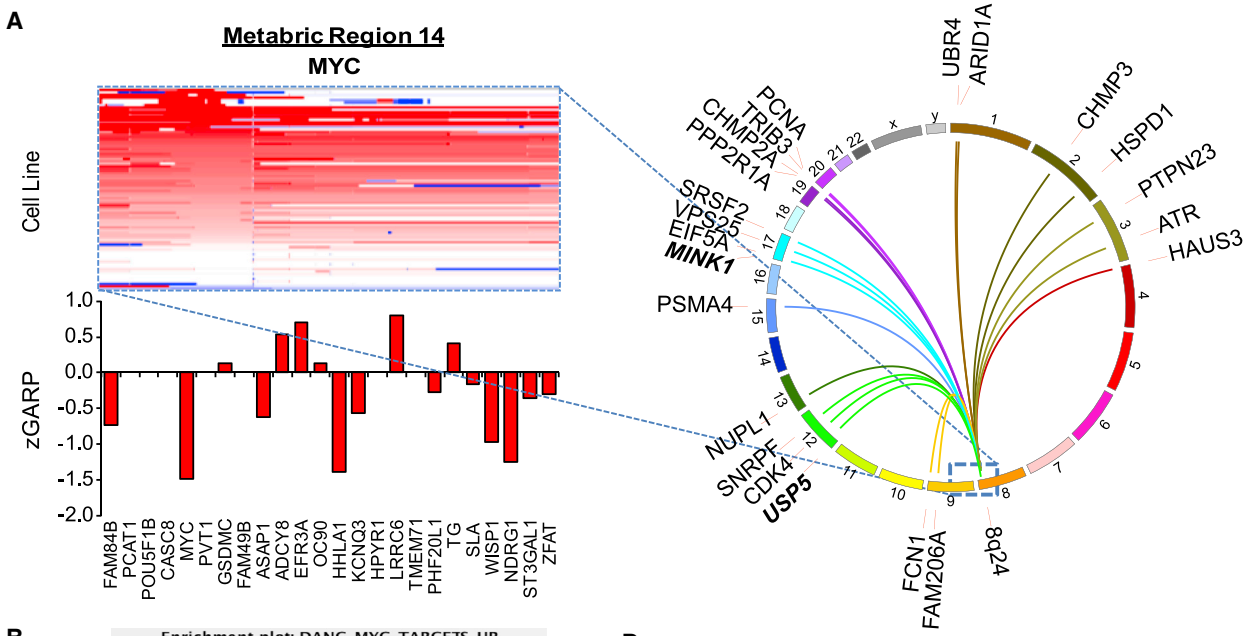

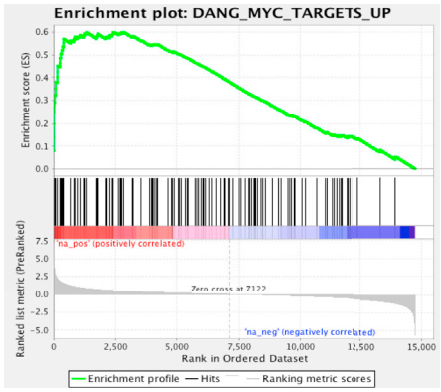

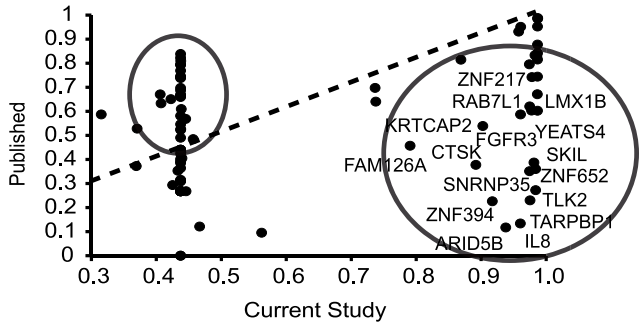

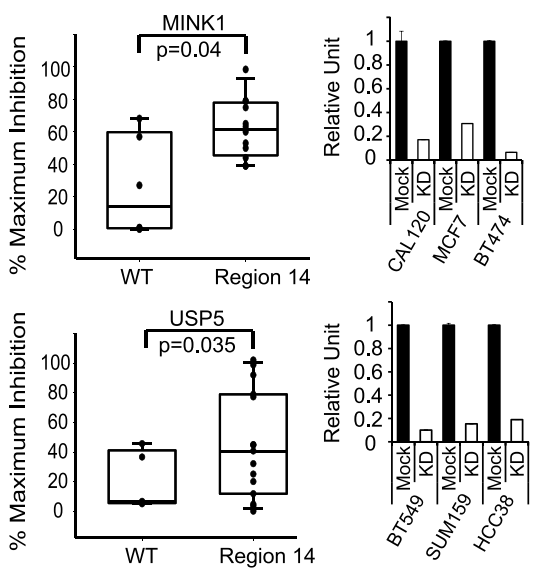

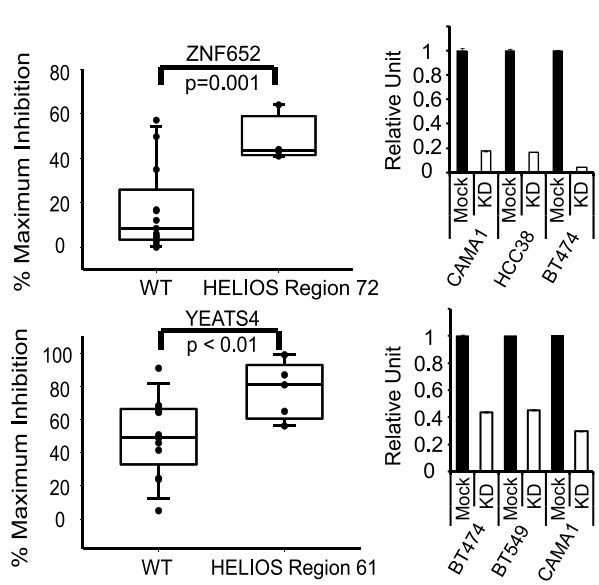

(legend on next page)

Functional Genomic Clustering Reveals Groups Not Captured by Expression Profiling

Using NMF clustering, we grouped lines based on shared dependencies ("functional genomic clustering") (Marcotte et al., 2012). Six "functional clusters" (fClusters) were observed, two containing lines designated as basal by expression profiling (fCluster-4 and fCluster-5), two luminal/HER2 clusters (fCluster-2 and fCluster-6), and two (fCluster-1 and fCluster-3) comprising a mix of basal and luminal/HER2 lines (Figure 5A). Thus, as we saw earlier (Marcotte et al., 2012), "basal" and "luminal/HER2" lines have distinct patterns of gene dependency. Yet, while there was little additional separation in our earlier study, with our expanded panel, HER2 (mainly fCluster-2) and ER^+ (fCluster-6) lines largely segregated into distinct fClusters. Genes determining the ER^+ (fCluster-6), $HER2^+$ (fCluster-2), and basal (fCluster-4) clusters (Table S5A) overlapped substantially with luminal-, HER2A-, or basal- essential genes, respectively (Figure 3). fCluster-1 was enriched for genes curated as H3K27-trimethylated, neuroactive peptides, or as involved in cytokine-cytokine interactions. fCluster-3 was enriched for annotations for cell cycle (G1/S and mitosis), DNA replication, and immune system genes, whereas fCluster-5 was enriched for genes involved in the immune system, lipid metabolism, and NGF signaling (Table S5A).

Drug Sensitivity and Gene Essentiality

We also compared gene essentiality and sensitivity data for 90 drugs tested against 84 breast cancer lines (Daemen et al., 2013), most of which (69) were included in our panel. Using siMEM, we identified genes whose essentiality correlated with sensitivity to mTOR/PI3K/ERBB2/AKT or EGFR/MEK/ERK inhibitors. Hierarchical clustering revealed distinct positive (red) and negative (blue) correlation clusters associated with drug sensitivity (Figure 5B; Supplemental Experimental Procedures). Reassuringly, genes for PI3K/AKT pathway components were required in lines sensitive to the cognate inhibitors. Sensitivity also correlated with essentiality of the luminal markers *ESR1*, *FOXA1*, and *GATA3*, consistent with the known sensitivity of luminal tumors to these agents. Likewise, EGFR/MEK/ERK inhibitor response correlated with sensitivity to *EGFR*, *GRB2*, *SOS1*, *MAPK1*, *MAPK3*, or *MAP2K1* depletion. Interestingly, response to EGFR/MEK/ERK inhibitors correlated with dependence on the NF-kB pathway: *RELA*, *REL*, and *NKAP* were more essential in such cells. These results comport with reports of NF-kB activation in response to EGFR, RAS, RAF, or MEK activation (Pan and Lin, 2013) and suggest that NF-kB inhibitors might be effective in basal breast cancer.

Drug sensitivity/essentiality comparisons also identified negative regulatory/tumor suppressor pathways. For example, *PTEN* was more essential in lines that were insensitive to mTOR/PI3K/ERBB2/AKT or EGFR/MEK/ERK inhibitors, consistent with the effects of PTEN deletion/inactivation (Worby and Dixon, 2014). Likewise, *MDM2* and *TP53* essentiality were associated with sensitivity or resistance to Nutlin-3A treatment, respectively.

Unsupervised analysis of the whole gene essentiality/drug sensitivity dataset revealed five clusters. Most drugs with a similar mechanism of action fell into the same cluster, and pathway analysis confirmed that essentiality clusters were enriched for genes implicated in the pathways targeted by their respective agents (Figure S5A; Tables S5B and S5C). Unanticipated clusters also emerged. For example, sensitivity to 11 drugs, which included alkylating agents, topoisomerase inhibitors, and cell cycle/cell cycle checkpoint inhibitors, correlated with essentiality of genes "associated with the H3K27me3 mark" (e.g., *PRDM13*, *NKX2-5*, *HOXC8*, *PAX7*, *HES2*) and for "neuropeptides and neurotransmitter signaling" (Figures S5B, box 2, S5C, and S5D). Notably, we had validated one of these genes, *HOXC8*, in our siRNA assays (Figures 3B and 3C).

Screen/drug sensitivity data might suggest drug combinations to kill resistant cells and/or negative regulators associated with drug resistance. For example, drugs targeting the PI3K/mTOR pathway (Cluster-1) strongly anti-correlated with *BCL2L1* essentiality (i.e., cell lines resistant to PI3K/mTOR inhibitors required *BCL2L1*). Interestingly, drug combinations targeting the PI3K/mTOR pathway and BCL-X_L are reported for several malignancies (Muranen et al., 2012; Rahmani et al., 2013). Another known combination predicted by our data is EGFR plus HDAC inhibitors (Zhang et al., 2015). Suggested combinations awaiting validation include RAF/MEK and CDK4 inhibitors, EGFR inhibitors with Cluster-5 drugs, BET-Is with Cluster-4 drugs, especially epirubicin and vinorelbine, PLK1 inhibitors with Nutlin-3A or PI3K/AKT inhibitors or Nutlin-3A with Cluster-5 drugs (Table S5B).

We also used DGIdb to identify essential genes that are potentially "druggable" (Griffith et al., 2013). Genes for kinases, phosphatases, and histone modifying enzymes were the most frequently essential, although other categories were represented (Figure 5C; Table S5D). Inhibitors exist for only a small fraction of most potential targets, especially the histone modifiers; a larger percentage of essential kinases had a known inhibitor (Figures 5C, 5D, and S5E).

Figure 4. *cis*- and *trans*-Essential Genes for CNAs

(A) Heatmap showing 8q24 amplification (METABRIC-14, containing *MYC*) in cell lines. Red, amplification; blue, deletion. Bar graph shows average zGARP score for genes in the amplified region in $amplicon^+$ lines. CIRCOS plot depicts top 20 significant genes (by siMEM) in $amplicon^+$ versus $amplicon^-$ cells.

(B) GSEA of *trans*-essential genes for MYC targets (FDR < 0.0001).

(C) Validation of 8q24 *trans*-essential genes with siRNAs. y axis, % maximum inhibition; bar graphs, knockdown efficiency (by qRT-PCR) of siRNAs.

(D) Correlation between published HELIOS scores (y axis) (Sanchez-Garcia et al., 2014) and new scores (x axis) obtained using our screen data. Circled genes deviate from earlier score and represent potential new amplified drivers.

(E) Validation of HELIOS genes with siRNAs. y axis, % maximum inhibition; bar graphs, knockdown efficiency of siRNAs. P values were calculated by one-sided t test.

See also Figure S4 and Table S4.

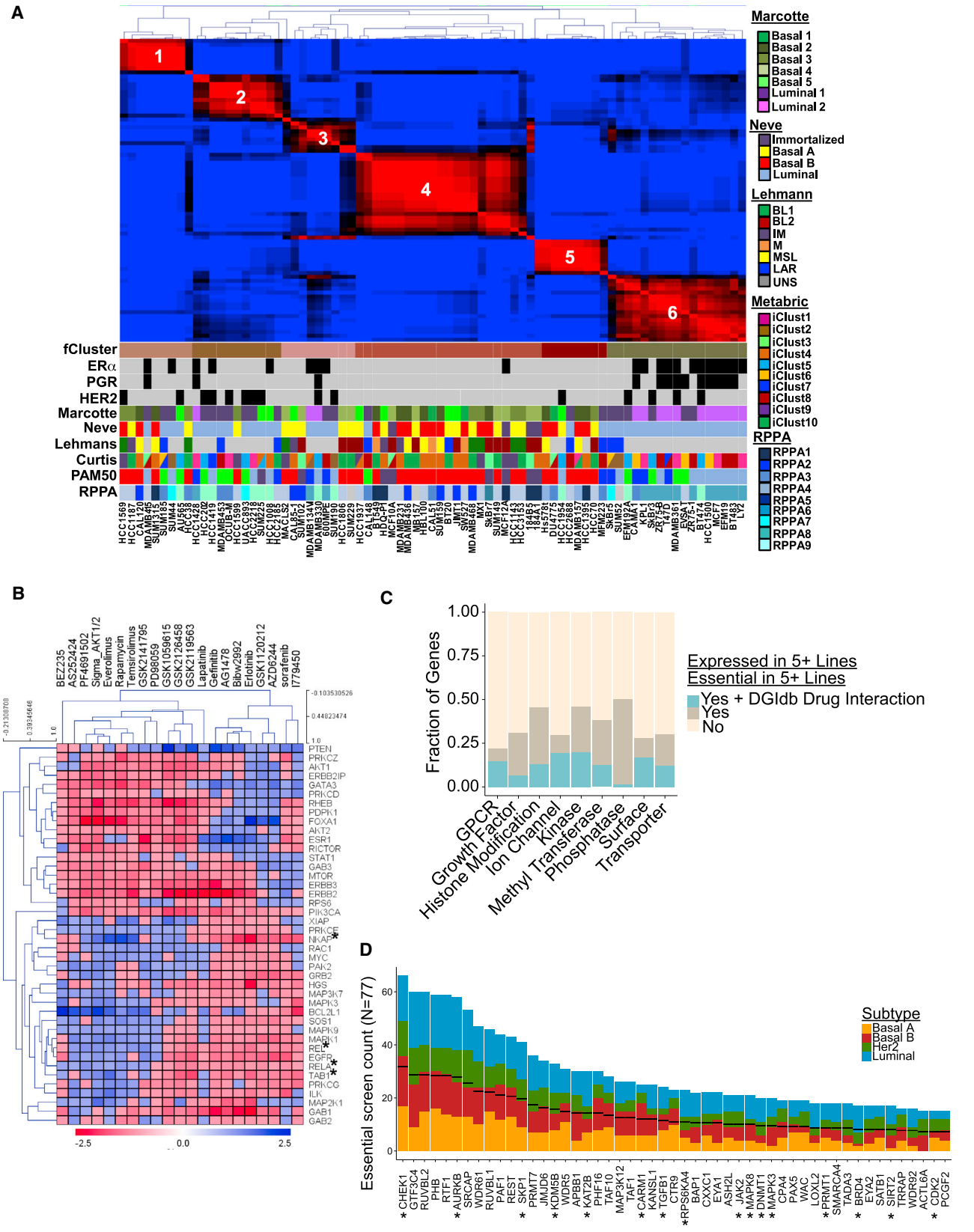

(legend on next page)

Additional Functional Genomic Properties of Cancer Cells

For most genes, essentiality decreased as expression increased (Figure 6A, right); such genes are enriched for housekeeping functions (Table S6A). A smaller set of genes became more essential with increased expression (Figure 6A, left): 16 of the 20 top-ranked genes in this group are known drivers in breast or other cancers (Table S6B). We suspected that other genes whose essentiality increased with increased expression might be drivers and tested several using siRNAs (Figures 6B and S6A). Indeed, 11/20 (55%) were more essential in lines with increased expression ($R > 0.3$). Genes more essential with increased expression showed lower expression overall than genes whose essentiality lessened with increased expression (Figure S6B). The former were more variably expressed, although, consistent with the behavior of known oncogenes (e.g., *ESR1*, *ERBB2*).

"CYCLOPS" (Nijhawan et al., 2012) and "GO" (Solimini et al., 2012) genes show increased essentiality upon heterozygous deletion of their cognate genomic regions. We identified 224 genes (FDR < 0.2) that were more essential with copy number loss (Figure 6C; Table S6C); their essentiality also correlated strongly with decrease in their expression (Figure 6D; Spearman $\rho = 0.74$). These genes overlapped significantly with CYCLOPS and GO genes, only five showed homozygous deletion in any line, and their protein products were enriched for housekeeping functions (Figure S6C; Table S6C; Supplemental Experimental Procedures). Thus, our data validate the CYCLOPS/GO concept and provide many other candidate members of this class of genes.

PIK3CA Mutations Drive Resistance to BET-I

BRD4, encoding a BET bromodomain-containing co-activator (Shi and Vakoc, 2014), was preferentially essential in luminal/HER2 lines (Figure 7A; Table S3G). Moreover, luminal/HER2 lines were more sensitive to *BRD4* depletion by siRNAs (Figures 7B and S7B), and expression of shRNA-resistant *BRD4* cDNA abrogated inhibition by *BRD4* shRNA (Figure S7C).

We tested the BET domain inhibitor (BET-I) JQ1 on a subset of our lines, expecting greater sensitivity in luminal/HER2 cells. Cell line GI50s ranged from low nM (<100) to μM (>2.5), with lines that showed high JQ1 sensitivity undergoing apoptosis, while resistant lines had slower cell-cycle progression (Figures S7D–S7F). However, many luminal/HER2 lines sensitive to *BRD4* knockdown were JQ1-resistant. By contrast, most basal lines that were sensitive to *BRD4* knockdown were JQ1-sensitive (Figure 7C; data not shown). In contrast to previous studies (Shi and Vakoc, 2014), JQ1 sensitivity did not reflect impaired *MYC* expression: sensitive and resistant cell lines displayed similar decreases in *MYC* mRNA (Figure S7G), and exogenous MYC did not convert JQ1-sensitive lines to JQ1-resistance (Figures S7H and S7I).

Instead, integrative analysis revealed a strong correlation between JQ1 resistance and *PIK3CA* mutation (Figure 7C). Overexpression of wild-type or mutant *PIK3CA* conferred JQ1 resistance on JQ1-sensitive SkBR3 cells (Figure 7D), establishing a causal relationship between PI3K and resistance. Moreover, A66, a PIK3CA-specific inhibitor, but not TGX-221 (PIK3CB-specific), increased the JQ1 sensitivity of resistant cells, as did the mTOR inhibitors rapamycin or Torin (Figures 7E and 7F). The one basal line (SUM159) sensitive to *BRD4* depletion but JQ1-resistant also has a *PIK3CA* mutation, and PIK3CA inhibitor treatment sensitized these cells to JQ1 (Figure S7J). Finally, combining JQ1 and Everolimus enhanced their respective antitumor effects (Figure 7G). In concert, these data indicate that BRD4 has bromodomain (BrD)-dependent and BrD-independent effects in breast cancer cells and establishes *PIK3CA* mutations as a BET-I resistance mechanism.

DISCUSSION

Most dropout screens analyze relatively few lines of any single cancer histotype. By contrast, we provide gene essentiality data for a large set of breast cancer lines with genomic, proteomic, and drug response annotation, and an analytic tool, siMEM, that more precisely measures differential essentiality. Our results identify and provide initial validation of synthetic lethal relationships with expression subtypes and CNAs, yield insight into essential pathways that correlate with anti-cancer drug response, and reveal general features of functional genomic screens. Illustrating the utility of combining genomic/functional genomic data, we identify and validate *BRD4* as a luminal/HER2-selective essential gene, uncover BET-independent requirements for BRD4 in luminal/HER2 cells, and reveal *PIK3CA* mutations as a potential resistance mechanism to BET-Is in vitro and in vivo.

The breadth of our screen has several advantages. Many have argued that breast cancer lines only partly reflect tumor heterogeneity (Hollestelle et al., 2010; Kao et al., 2009; Neve et al., 2006). But there are at least ten breast cancer subtypes (Curtis et al., 2012; Lehmann et al., 2011; Cancer Genome Atlas Network, 2012); only a large panel could possibly represent such heterogeneity (Figures 1 and S1). Our screen identified nearly all known breast cancer drivers linked to the appropriate biomarker (Figures 3A, 4A, and S4A). The increased power of our dataset also revises the identification of putative targets of

Figure 5. Screen Refines Classification and Pathway Identification

(A) NMF clustering of screen results (zGARP). *ESR1*, *ERBB2*, and *PGR* expression are shown by black squares. Colored boxes indicate major published subcategories.

(B) Unsupervised analysis of essential genes implicated in PI3K/mTOR or EGFR/MEK/ERK pathways. Heatmap shows association of essentiality for each gene (this study) with sensitivity to drugs targeting these pathways (Daemen et al., 2013). The asterisk (*) indicates genes belonging to the NF-κB pathway.

(C) Fraction of essential genes overlapping with reported "druggable" gene categories or gene-drug interactions (DGIdb).

(D) Top-ranked histone-modifying enzymes deemed essential in our screen, by breast cancer subtype. *Reported gene-drug interaction in DGIdb. Black lines represent 50% of lines in which the gene is essential.

See also Figure S5 and Table S5.

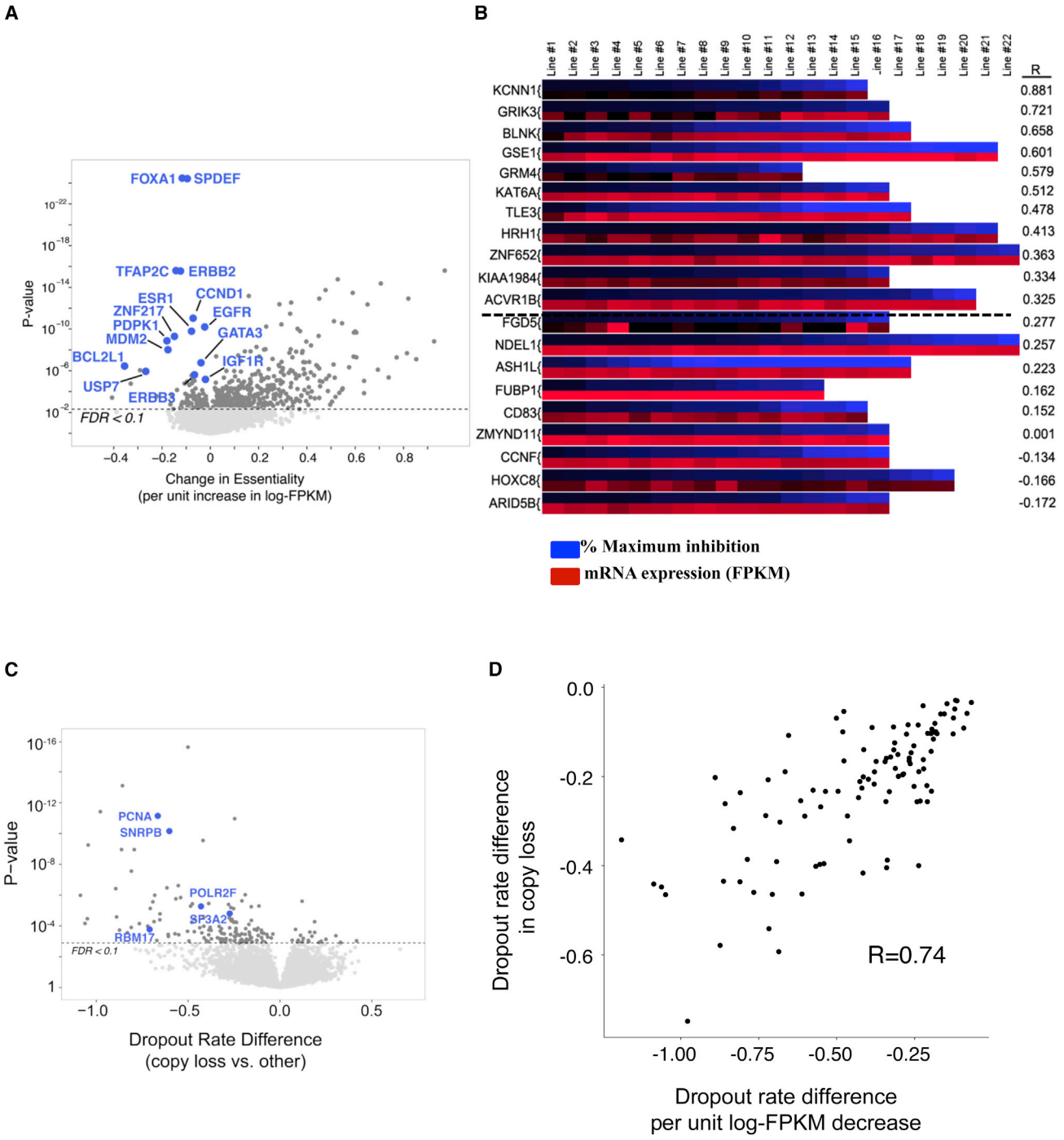

Figure 6. Additional Features of shRNA Screens

(A) Volcano plot of relationship between essentiality and gene expression. x axis, change in dropout rate per unit increase in expression log-FPKM; y axis, p value.

(B) Heatmap showing % inhibition of proliferation following knockdown by siRNA in cell lines. For each gene, the upper row (blue) represents maximum growth inhibition, while the lower row (red) represents mRNA levels of the same gene in each line. R, Pearson correlation.

(C) Vulnerabilities associated with genomic loss (CYCLOPS genes).

(D) Strong agreement (Spearman $\rho = 0.74$, p value $< 2.2 \times 10^{-16}$) between genes more essential with heterozygous loss (FDR < 0.25) and genes whose essentiality changes significantly with expression (FDR < 0.25).

See also Figure S6 and Table S6.

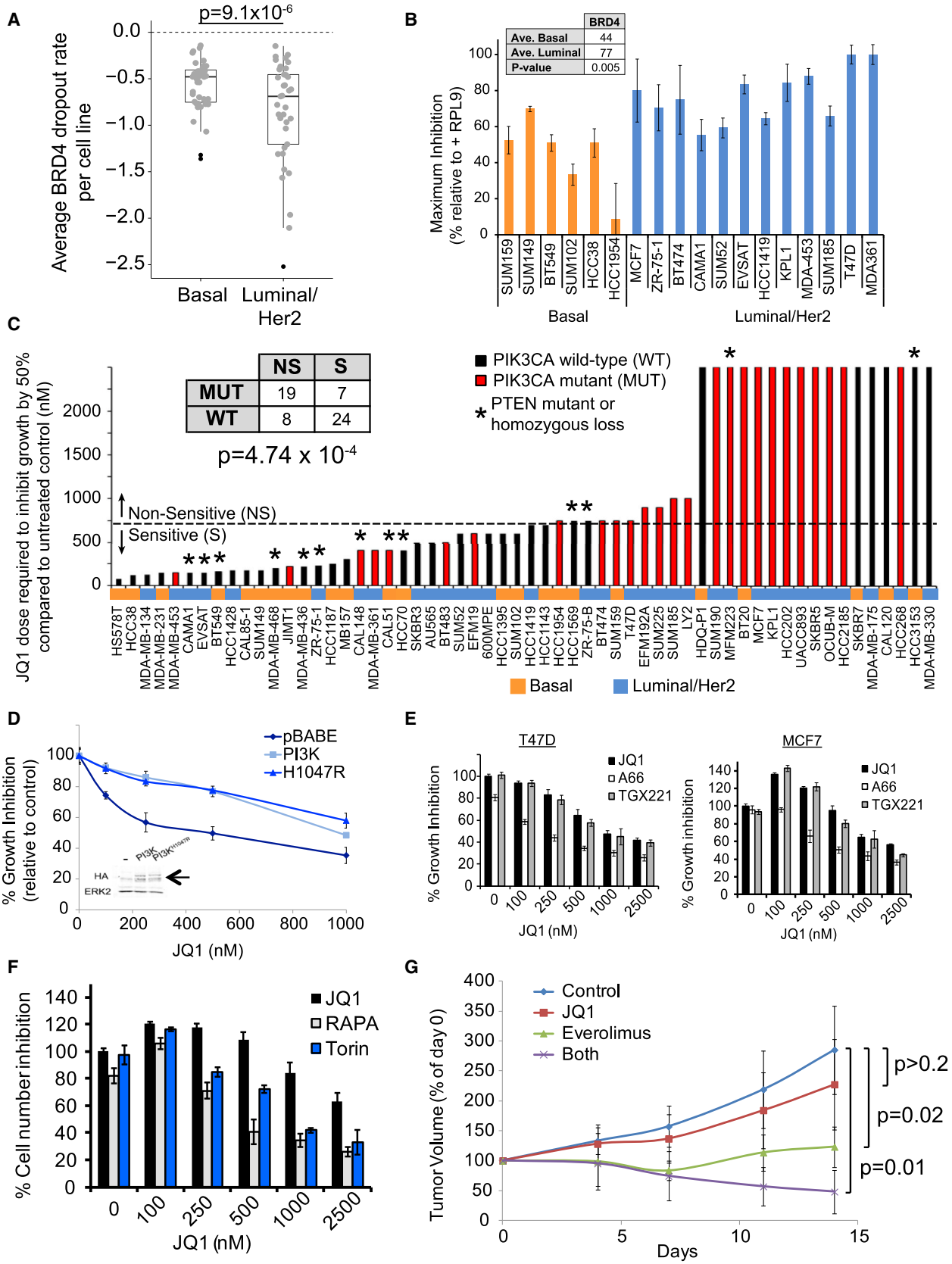

(legend on next page)

some breast cancer amplicons and strengthens the identification of others by HELIOS (Figure 4D; Table S4E). Thus, if enough cell lines are tested, they provide valid surrogates for probing core cancer cell properties, such as proliferation/survival.

Conventional algorithms for sh/siRNA screens generate hairpin-level and/or gene-level scores that summarize multiple measurements and fail to identify known differential essential genes. By contrast, siMEM greatly improves detection of essentials associated with CNAs, gene expression, somatic mutations, or cancer subtype without increasing the false positive rate. "Hits" suggested by siMEM have a high validation rate (~60%–70%) (Figures 3B and 6B), and an analogous approach can be applied to any pooled screen (e.g., CRISPR/Cas9 screens).

Our screen identified "general" and "context-specific" essentials. As expected, general essentials are enriched for housekeeping functions, yet some show a gradient of essentiality tied to specific genetic parameters. For example, specific splicing factors (data not shown, but see Hsu et al., 2015) and proteasome genes are preferentially required in basal lines (Table S3F). A splicing inhibitor is in clinical trials (E7107; NCT00459823), and several proteasome inhibitors are approved drugs (Dou and Zonder, 2014) and could be repurposed for breast cancer therapy.

Our data provide strong confirmation of earlier work suggesting distinct subtype-specific vulnerabilities. The pivotal roles of hormone receptors in luminal breast cancer, of ERBB2 signaling in $HER2^+$ disease, and of EGFR and WNT signaling in basal breast cancer are confirmed by our screen hits (Figures 3A, 3D, and 3E; Tables S3F and S3G). We also identify several "druggable" targets, including *EFNB3/EPHA4*, *MAP2K4*, *MAPK13*, and *IL32*, for basal breast cancer, the most lethal form of the disease. How these genes promote basal breast cancer is unclear. EFNB3/EPHA4 are a ligand/receptor pair that promotes neuronal proliferation and survival (Furne et al., 2009; Takemoto et al., 2002). MAP2K4 phosphorylates and activates MAPK13 (O'Callaghan et al., 2014); MAPK13 and IL32 are linked to IL-1 signaling (Netea et al., 2005; Yousif et al., 2013), which also is basal-specific in our screen. Basal A cells are preferentially susceptible to *CAND1-NEDD8* depletion. A NEDD8 inhibitor, MLN4924, is in phase 1 trials (NCT00677170, NCT01862328); TNBC patients might benefit from this agent.

Basal B cell lines are claudin-low-like, represent a unique TNBC subset, and have EMT-like, cancer stem cell-like, and mammary stem cell-like gene signatures (Lim et al., 2010), like those seen in chemotherapy-resistant cells (Creighton et al., 2009). Basal B lines also showed unique essentialities: basal B-essentials are enriched for motility, immune-related, developmental and neuronal, and cell junction and adhesion genes, several of which validate in siRNA experiments (Figure 3B). We also find marked functional similarity between basal breast cancer and HGSC (Figure S3C). Our results and the shared genomics of these tumors (Cancer Genome Atlas Research Network, 2011; Cancer Genome Atlas Network, 2012) argue for similar treatment strategies and drug discovery efforts.

Consistent with earlier work (Davoli et al., 2013; Solimini et al., 2012), our results suggest that for many amplicons, multiple genes contribute to increased fitness. For some amplicons, no clear *cis*-essential gene was identified. Failure to identify such genes might be technical (e.g., insufficient $amplicon^+$ lines). More likely, these amplicons select for multiple weak drivers, miRNAs/long non-coding RNAs (lncRNAs), or genes dispensable for proliferation/survival, but mediating other cancer hallmarks. For other amplicons, the key gene(s) cannot be targeted directly, nor can deleted tumor suppressor genes be restored. "*trans*-Essentials" provide insight into pathways perturbed by CNAs and can suggest more tractable drug targets. For example, METABRIC region 14, containing *MYC*, confers dependency on a MYC-regulated functional network. Two genes in this network, *MINK1* and *USP5*, are potential drug targets and validate by siRNA. Potentially druggable *trans*-associations also exist for common deletions: e.g., *RB1*-deleted lines are more sensitive to *MAP2K2* depletion, whereas *CDKN2A*-deleted lines rely more on *KAT6B*, *ADRBK1*, *SYK*, and *DNMT3A.*

As expected, genes encoding targets of known anti-cancer drugs are more essential in lines sensitive to those agents. But other genes, without known or obvious connections to the target pathway, also show essentiality strongly correlated with specific drug sensitivity. Also, gene essentiality can anti-correlate with drug sensitivity. Such genes might mediate therapy resistance and suggest potential combination strategies.

BRD4 was implicated in cancer by studies of NUT midline carcinoma, which often harbors a *BRD4-NUT* translocation (French et al., 2003). Subsequently, BRD4 emerged as a potential target for many other neoplasms (Shi and Vakoc, 2014). We identified *BRD4* as more essential in luminal/HER2 lines (Figures 7A and 7B; Table S3G). In hematologic malignancies, BET-I sensitivity

Figure 7. *BRD4* Is Luminal-Essential, and *PIK3CA* Mutations Cause BET-I Resistance

(A) Box plot showing *BRD4* dropout in each line, by subtype.

(B) *BRD4* siRNAs confirm pooled screen results. Averages are maximum percent inhibition ($p = 0.005$, Student's t test).

(C) Effect of JQ1 on breast cancer lines. Table (inset) shows number of lines, grouped by JQ1 sensitivity (NS, non-sensitive; S, sensitive) and *PIK3CA* status (mut, mutated; WT, wild-type). Red shading shows lines with *PIK3CA* mutations. Mutant lines were more likely to be JQ1-resistant ($p < 4.7 \times 10^{-4}$, chi-square test). Sensitive lines have GI50 < 750 nM. *Lines with *PTEN* mutation/homozygous deletion.

(D) WT or mutant *PIK3CA* (H1047R) renders JQ1-sensitive SkBr3 line resistant to JQ1. Inset: immunoblot showing expression of PIK3CA-p110α. Arrow indicates the specific band.

(E) JQ1 cooperates with PIK3CA (A66; 1 μM), but not with PIK3CB (TGX; 1), inhibitors to decrease MCF7 and T47D proliferation. "0" JQ1 represents A66 or TGX alone.

(F) JQ1 cooperates with mTOR inhibitors (rapamycin; 0.5 nM, Torin; 50 nM) to decrease MCF7 proliferation. "0" represents rapamycin or Torin alone.

(G) JQ1 and Everolimus cooperatively inhibit xenograft growth. MCF7 cells (2×10^6) were injected into mammary fat pads of athymic nude mice bearing a slow release estrogen pellet. When tumors were 5 × 5 mm (~21 days), mice were grouped into: (1) control, (2) JQ1 (50 mg/kg/day intraperitoneally [IP]), (3) Everolimus (5 mg/kg/day by gavage), and (4) JQ1 + Everolimus daily. Tumors were measured with calipers every 3–4 days. P value, one-sided Student's t test.

See also Figure S7.

correlates with *MYC* downregulation and is antagonized by exogenous *MYC* expression (Shi and Vakoc, 2014). Very recently, mouse basal-like breast tumors caused by *MYC* overexpression and mutant *PIK3CA* were found to be sensitive to combined BET/PI3K inhibition, as was a human basal line, SUM159 (Stratikopoulos et al., 2015). However, we saw no correlation between JQ1 sensitivity and basal *MYC* levels or the ability of JQ1 to inhibit *MYC* expression. Nor does forced *MYC* expression alter JQ1 sensitivity (Figures S7G–S7I).

Instead, using our genomic data, we found that *PIK3CA* mutations are biomarkers of BET-I resistance. Moreover, they are functional biomarkers, as treating cell lines or xenografts with a BET-I/mTOR inhibitor combination improves efficacy (Figures 7F and 7G). Our results have clear clinical implications, as Everolimus is approved for ER^+ breast cancer, and BET-Is are in clinical trials. *PIK3CA* mutations are most frequent in luminal tumors, so such patients would likely benefit most from BET-I/mTOR-I combinations. But our results and those of Stratikopoulos et al. (2015) also suggest a role for BET-Is as single agents in basal tumors. Surprisingly, and for unclear reasons, in basal lines, *PTEN* mutation/homozygous deletion predicts BET-I sensitivity (Figure 7C; data not shown).

Finally, as breast cancer lines can be JQ1-insensitive, but *BRD4*-dependent, BRD4 must have (a) BRD-independent function(s). Although the detailed mechanism is unclear, mutant *PIK3CA* confers JQ1-resistance, so PI3K pathway activation can selectively abrogate BRD-dependent, but not BRD-independent functions of BRD4. Thus, our integrated functional genomic approach not only can suggest new treatment strategies for breast tumor subtypes, but also reveals new features of breast cancer biology.

EXPERIMENTAL PROCEDURES

For additional details and computational methods, see Supplemental Experimental Procedures.

Cell Lines

Cell lines were from the American Type Culture Collection (ATCC), Asterands, Deutsche Sammlung von Mikroorganismen und Zellkultrenen GmbH (DSMZ), or were available in-house (Table S1).

Genomics/Proteomics

SNP-Arrays

Genomic DNA was amplified with the Illumina Infinium Genotyping kit, hybridized to Human Omni-Quad Beadchips, and analyzed on an iScan (Illumina). Data were quantified in GenomeStudio Version 2010.2 (Illumina) using Omni-Quad Multiuse_H manifest (April 2011 release), containing data from GenomeBuild 37, Hg19.

RNA-Seq

RNA was reverse transcribed using the Illumina TruSeq Stranded mRNA kit. Libraries were sized (Agilent Bioanalyzer), normalized, and pooled (six each), and loaded onto an Illumina cBot. Paired-end sequencing (50 cycles) was performed on an Illumina HiSeq 2000.

Targeted Sequencing

DNA for 126 genes (1.264 Mbp) mutated at $\geq$3% frequency in breast or ovarian carcinoma was captured using Agilent SureSelect XT, loaded onto the cBot, and subjected to paired-end sequencing (100 cycles).

miRNA

miRNA expression was assessed by using the nCounter Human V2 miRNA Assay Kit (Cat# GXA-MIR2-48) and a NanoString counter.

RPPA

RPPAs were generated and analyzed as described (Tibes et al., 2006). For all lines, fresh media was added at 80%–90% confluency, and cells were harvested 16 hr later.

shRNA/siRNA Experiments

Pooled screens with the TRC-II library were performed as described (Marcotte et al., 2012). HCC712, ZR-75-30, MDA-MB-175VII, UACC812, and UACC3199 failed quality control. For validation, cells (1,000–3,000) seeded in 96-well plates for 24 hr were transfected with Dharmacon SMARTPOOL siRNAs (10 nM) using Lipofectamine RNAimax (Life Technologies). After 7 days, cells were stained with Alamar blue (Life Technologies), which measures redox activity and is as a surrogate for cell number. Percent maximum inhibition, corrected for transfection efficiency, was determined using siRNAs for the general essential *RPL9*.

Xenografts

MCF7 cells (5×10^6) were mixed 1:1 with growth factor-reduced Matrigel (BD Biosciences) and injected into mammary fat pads of athymic nude mice (Charles River). When tumors were 5 × 5 mm, mice were separated into control and drug-treated groups. JQ1 was synthesized (Filippakopoulos et al., 2010). Everolimus was purchased from Selleckchem.

RNA-seq and screen data are deposited in Gene Expression Omnibus (GEO: GSE73526 and GEO: GSE74702). Genomics and proteomics data are available at http://neellab.github.io/bfg/. All code is available upon request from A.S. and siMEM code will be posted at http://neellab.github.io/simem/.

All animal studies were approved by the University Health Network Animal Care Committee, under Animal Use Protocol (#1239).

ACCESSION NUMBERS

The accession numbers for the RNA-seq and screen data reported in this paper are Gene Expression Omnibus (GEO): GSE73526 and GSE74702.

SUPPLEMENTAL INFORMATION

Supplemental Information includes Supplemental Experimental Procedures, seven figures, and six tables and can be found with this article online at http://dx.doi.org/10.1016/j.cell.2015.11.062.

AUTHOR CONTRIBUTIONS

R.M., A.S., J.M., and B.G.N. designed the study. R.M. and M.H. performed experiments. G.B.M. performed RPPAs. A.S. designed/implemented siMEM with input from J.M. and K.R.B. K.R.B., C.V., R.M., and A.S. performed genomic and statistical analyses. J.R. and G.D.B. performed pathway enrichment and PPI analyses. F.S.G. and D.P. implemented HELIOS. J.B. provided JQ1. R.M., A.S., and B.G.N. wrote the paper with help from all authors.

ACKNOWLEDGMENTS

This work was supported by the Canadian Foundation for Innovation (J.M.) and the Ontario Research Fund (B.G.N. and J.M.). B.G.N. was a Canada Research Chair, Tier 1, and work in his laboratory was supported in part by the Princess Margaret Cancer Foundation. R.M. was partly funded by a postdoctoral fellowship from the Canadian Breast Cancer Foundation. This work was also supported by NIH grants R37 CA49132 (B.G.N.), P41 GM103504, R01 GM070743, U41 HG006623 (G.D.B.), and PO1 CA099031 (G.B.M.), a Komen SAC and Promise grant (G.B.M.), and the M.D. Anderson CCSG functional proteomics core (CA16672).

Received: July 27, 2015
Revised: October 9, 2015
Accepted: November 23, 2015
Published: January 14, 2016

REFERENCES

Banerji, S., Cibulskis, K., Rangel-Escareno, C., Brown, K.K., Carter, S.L., Frederick, A.M., Lawrence, M.S., Sivachenko, A.Y., Sougnez, C., Zou, L., et al. (2012). Sequence analysis of mutations and translocations across breast cancer subtypes. Nature *486*, 405–409.

Barbie, D.A., Tamayo, P., Boehm, J.S., Kim, S.Y., Moody, S.E., Dunn, I.F., Schinzel, A.C., Sandy, P., Meylan, E., Scholl, C., et al. (2009). Systematic RNA interference reveals that oncogenic KRAS-driven cancers require TBK1. Nature *462*, 108–112.

Bosher, J.M., Williams, T., and Hurst, H.C. (1995). The developmentally regulated transcription factor AP-2 is involved in c-erbB-2 overexpression in human mammary carcinoma. Proc. Natl. Acad. Sci. USA *92*, 744–747.

Buchwalter, G., Hickey, M.M., Cromer, A., Selfors, L.M., Gunawardane, R.N., Frishman, J., Jeselsohn, R., Lim, E., Chi, D., Fu, X., et al. (2013). PDEF promotes luminal differentiation and acts as a survival factor for ER-positive breast cancer cells. Cancer Cell *23*, 753–767.

Cancer Genome Atlas Network (2012). Comprehensive molecular portraits of human breast tumours. Nature *490*, 61–70.

Cancer Genome Atlas Research Network (2011). Integrated genomic analyses of ovarian carcinoma. Nature *474*, 609–615.

Cheung, H.W., Cowley, G.S., Weir, B.A., Boehm, J.S., Rusin, S., Scott, J.A., East, A., Ali, L.D., Lizotte, P.H., Wong, T.C., et al. (2011). Systematic investigation of genetic vulnerabilities across cancer cell lines reveals lineage-specific dependencies in ovarian cancer. Proc. Natl. Acad. Sci. USA *108*, 12372–12377.

Cortez, D., Wang, Y., Qin, J., and Elledge, S.J. (1999). Requirement of ATM-dependent phosphorylation of brca1 in the DNA damage response to double-strand breaks. Science *286*, 1162–1166.

Creighton, C.J., Li, X., Landis, M., Dixon, J.M., Neumeister, V.M., Sjolund, A., Rimm, D.L., Wong, H., Rodriguez, A., Herschkowitz, J.I., et al. (2009). Residual breast cancers after conventional therapy display mesenchymal as well as tumor-initiating features. Proc. Natl. Acad. Sci. USA *106*, 13820–13825.

Curtis, C., Shah, S.P., Chin, S.F., Turashvili, G., Rueda, O.M., Dunning, M.J., Speed, D., Lynch, A.G., Samarajiwa, S., Yuan, Y., et al.; METABRIC Group (2012). The genomic and transcriptomic architecture of 2,000 breast tumours reveals novel subgroups. Nature *486*, 346–352.

Daemen, A., Griffith, O.L., Heiser, L.M., Wang, N.J., Enache, O.M., Sanborn, Z., Pepin, F., Durinck, S., Korkola, J.E., Griffith, M., et al. (2013). Modeling precision treatment of breast cancer. Genome Biol. *14*, R110.

Dang, C.V. (2012). MYC on the path to cancer. Cell *149*, 22–35.

Davoli, T., Xu, A.W., Mengwasser, K.E., Sack, L.M., Yoon, J.C., Park, P.J., and Elledge, S.J. (2013). Cumulative haploinsufficiency and triplosensitivity drive aneuploidy patterns and shape the cancer genome. Cell *155*, 948–962.

Dhillon, S. (2015). Palbociclib: first global approval. Drugs *75*, 543–551.

Dou, Q.P., and Zonder, J.A. (2014). Overview of proteasome inhibitor-based anti-cancer therapies: perspective on bortezomib and second generation proteasome inhibitors versus future generation inhibitors of ubiquitin-proteasome system. Curr. Cancer Drug Targets *14*, 517–536.

Dvinge, H., Git, A., Gräf, S., Salmon-Divon, M., Curtis, C., Sottoriva, A., Zhao, Y., Hirst, M., Armisen, J., Miska, E.A., et al. (2013). The shaping and functional consequences of the microRNA landscape in breast cancer. Nature *497*, 378–382.

Ellis, M.J., Ding, L., Shen, D., Luo, J., Suman, V.J., Wallis, J.W., Van Tine, B.A., Hoog, J., Goiffon, R.J., Goldstein, T.C., et al. (2012). Whole-genome analysis informs breast cancer response to aromatase inhibition. Nature *486*, 353–360.

Filippakopoulos, P., Qi, J., Picaud, S., Shen, Y., Smith, W.B., Fedorov, O., Morse, E.M., Keates, T., Hickman, T.T., Felletar, I., et al. (2010). Selective inhibition of BET bromodomains. Nature *468*, 1067–1073.

Flick, K., and Kaiser, P. (2013). Set them free: F-box protein exchange by Cand1. Cell Res. *23*, 870–871.

French, C.A., Miyoshi, I., Kubonishi, I., Grier, H.E., Perez-Atayde, A.R., and Fletcher, J.A. (2003). BRD4-NUT fusion oncogene: a novel mechanism in aggressive carcinoma. Cancer Res. *63*, 304–307.

Furne, C., Ricard, J., Cabrera, J.R., Pays, L., Bethea, J.R., Mehlen, P., and Liebl, D.J. (2009). EphrinB3 is an anti-apoptotic ligand that inhibits the dependence receptor functions of EphA4 receptors during adult neurogenesis. Biochim. Biophys. Acta *1793*, 231–238.

Gatei, M., Scott, S.P., Filippovitch, I., Soronika, N., Lavin, M.F., Weber, B., and Khanna, K.K. (2000). Role for ATM in DNA damage-induced phosphorylation of BRCA1. Cancer Res. *60*, 3299–3304.

Griffith, M., Griffith, O.L., Coffman, A.C., Weible, J.V., McMichael, J.F., Spies, N.C., Koval, J., Das, I., Callaway, M.B., Eldred, J.M., et al. (2013). DGIdb: mining the druggable genome. Nat. Methods *10*, 1209–1210.

Guo, W., Keckesova, Z., Donaher, J.L., Shibue, T., Tischler, V., Reinhardt, F., Itzkovitz, S., Noske, A., Zürrer-Härdi, U., Bell, G., et al. (2012a). Slug and Sox9 cooperatively determine the mammary stem cell state. Cell *148*, 1015–1028.

Guo, Y., Chinyengetere, F., Dolinko, A.V., Lopez-Aguiar, A., Lu, Y., Galimberti, F., Ma, T., Feng, Q., Sekula, D., Freemantle, S.J., et al. (2012b). Evidence for the ubiquitin protease UBP43 as an antineoplastic target. Mol. Cancer Ther. *11*, 1968–1977.

Hart, T., Brown, K.R., Sircoulomb, F., Rottapel, R., and Moffat, J. (2014). Measuring error rates in genomic perturbation screens: gold standards for human functional genomics. Mol. Syst. Biol. *10*, 733.

Hennessy, B.T., Gonzalez-Angulo, A.M., Stemke-Hale, K., Gilcrease, M.Z., Krishnamurthy, S., Lee, J.S., Fridlyand, J., Sahin, A., Agarwal, R., Joy, C., et al. (2009). Characterization of a naturally occurring breast cancer subset enriched in epithelial-to-mesenchymal transition and stem cell characteristics. Cancer Res. *69*, 4116–4124.

Hollestelle, A., Nagel, J.H., Smid, M., Lam, S., Elstrodt, F., Wasielewski, M., Ng, S.S., French, P.J., Peeters, J.K., Rozendaal, M.J., et al. (2010). Distinct gene mutation profiles among luminal-type and basal-type breast cancer cell lines. Breast Cancer Res. Treat. *121*, 53–64.

Hsu, T.Y., Simon, L.M., Neill, N.J., Marcotte, R., Sayad, A., Bland, C.S., Echeverria, G.V., Sun, T., Kurley, S.J., Tyagi, S., et al. (2015). The spliceosome is a therapeutic vulnerability in MYC-driven cancer. Nature *525*, 384–388.

Jamdade, V.S., Sethi, N., Mundhe, N.A., Kumar, P., Lahkar, M., and Sinha, N. (2015). Therapeutic targets of triple-negative breast cancer: a review. Br. J. Pharmacol. *172*, 4228–4237.

Kao, J., Salari, K., Bocanegra, M., Choi, Y.L., Girard, L., Gandhi, J., Kwei, K.A., Hernandez-Boussard, T., Wang, P., Gazdar, A.F., et al. (2009). Molecular profiling of breast cancer cell lines defines relevant tumor models and provides a resource for cancer gene discovery. PLoS ONE *4*, e6146.

Kim, J.H., Hubbard, N.E., Ziboh, V., and Erickson, K.L. (2005). Attenuation of breast tumor cell growth by conjugated linoleic acid via inhibition of 5-lipoxygenase activating protein. Biochim. Biophys. Acta *1736*, 244–250.

König, R., Chiang, C.Y., Tu, B.P., Yan, S.F., DeJesus, P.D., Romero, A., Bergauer, T., Orth, A., Krueger, U., Zhou, Y., and Chanda, S.K. (2007). A probability-based approach for the analysis of large-scale RNAi screens. Nat. Methods *4*, 847–849.

Lehmann, B.D., Bauer, J.A., Chen, X., Sanders, M.E., Chakravarthy, A.B., Shyr, Y., and Pietenpol, J.A. (2011). Identification of human triple-negative breast cancer subtypes and preclinical models for selection of targeted therapies. J. Clin. Invest. *121*, 2750–2767.

Lim, E., Wu, D., Pal, B., Bouras, T., Asselin-Labat, M.L., Vaillant, F., Yagita, H., Lindeman, G.J., Smyth, G.K., and Visvader, J.E. (2010). Transcriptome analyses of mouse and human mammary cell subpopulations reveal multiple conserved genes and pathways. Breast Cancer Res. *12*, R21.

Lupien, M., Eeckhoute, J., Meyer, C.A., Wang, Q., Zhang, Y., Li, W., Carroll, J.S., Liu, X.S., and Brown, M. (2008). FoxA1 translates epigenetic signatures into enhancer-driven lineage-specific transcription. Cell *132*, 958–970.

Maire, V., Némati, F., Richardson, M., Vincent-Salomon, A., Tesson, B., Rigaill, G., Gravier, E., Marty-Prouvost, B., De Koning, L., Lang, G., et al. (2013). Polo-like kinase 1: a potential therapeutic option in combination with conventional

chemotherapy for the management of patients with triple-negative breast cancer. Cancer Res. *73*, 813–823.

Marcotte, R., Brown, K.R., Suarez, F., Sayad, A., Karamboulas, K., Krzyzanowski, P.M., Sircoulomb, F., Medrano, M., Fedyshyn, Y., Koh, J.L., et al. (2012). Essential gene profiles in breast, pancreatic, and ovarian cancer cells. Cancer Discov. *2*, 172–189.

Muranen, T., Selfors, L.M., Worster, D.T., Iwanicki, M.P., Song, L., Morales, F.C., Gao, S., Mills, G.B., and Brugge, J.S. (2012). Inhibition of PI3K/mTOR leads to adaptive resistance in matrix-attached cancer cells. Cancer Cell *21*, 227–239.

Netea, M.G., Azam, T., Ferwerda, G., Girardin, S.E., Walsh, M., Park, J.S., Abraham, E., Kim, J.M., Yoon, D.Y., Dinarello, C.A., and Kim, S.H. (2005). IL-32 synergizes with nucleotide oligomerization domain (NOD) 1 and NOD2 ligands for IL-1beta and IL-6 production through a caspase 1-dependent mechanism. Proc. Natl. Acad. Sci. USA *102*, 16309–16314.

Neve, R.M., Chin, K., Fridlyand, J., Yeh, J., Baehner, F.L., Fevr, T., Clark, L., Bayani, N., Coppe, J.P., Tong, F., et al. (2006). A collection of breast cancer cell lines for the study of functionally distinct cancer subtypes. Cancer Cell *10*, 515–527.

Nijhawan, D., Zack, T.I., Ren, Y., Strickland, M.R., Lamothe, R., Schumacher, S.E., Tsherniak, A., Besche, H.C., Rosenbluh, J., Shehata, S., et al. (2012). Cancer vulnerabilities unveiled by genomic loss. Cell *150*, 842–854.

O'Callaghan, C., Fanning, L.J., and Barry, O.P. (2014). p38δ MAPK: Emerging Roles of a Neglected Isoform. Int. J. Cell Biol. *2014*, 272689.

Pan, D., and Lin, X. (2013). Epithelial growth factor receptor-activated nuclear factor kappaB signaling and its role in epithelial growth factor receptor-associated tumors. Cancer J. *19*, 461–467.

Pao, G.M., Janknecht, R., Ruffner, H., Hunter, T., and Verma, I.M. (2000). CBP/p300 interact with and function as transcriptional coactivators of BRCA1. Proc. Natl. Acad. Sci. USA *97*, 1020–1025.

Parker, J.S., Mullins, M., Cheang, M.C., Leung, S., Voduc, D., Vickery, T., Davies, S., Fauron, C., He, X., Hu, Z., et al. (2009). Supervised risk predictor of breast cancer based on intrinsic subtypes. J. Clin. Oncol. *27*, 1160–1167.

Perou, C.M., Sørlie, T., Eisen, M.B., van de Rijn, M., Jeffrey, S.S., Rees, C.A., Pollack, J.R., Ross, D.T., Johnsen, H., Akslen, L.A., et al. (2000). Molecular portraits of human breast tumours. Nature *406*, 747–752.

Petrocca, F., Altschuler, G., Tan, S.M., Mendillo, M.L., Yan, H., Jerry, D.J., Kung, A.L., Hide, W., Ince, T.A., and Lieberman, J. (2013). A genome-wide siRNA screen identifies proteasome addiction as a vulnerability of basal-like triple-negative breast cancer cells. Cancer Cell *24*, 182–196.

Prat, A., Parker, J.S., Karginova, O., Fan, C., Livasy, C., Herschkowitz, J.I., He, X., and Perou, C.M. (2010). Phenotypic and molecular characterization of the claudin-low intrinsic subtype of breast cancer. Breast Cancer Res. *12*, R68.

Rahmani, M., Aust, M.M., Attkisson, E., Williams, D.C., Jr., Ferreira-Gonzalez, A., and Grant, S. (2013). Dual inhibition of Bcl-2 and Bcl-xL strikingly enhances PI3K inhibition-induced apoptosis in human myeloid leukemia cells through a GSK3- and Bim-dependent mechanism. Cancer Res. *73*, 1340–1351.

Riaz, M., van Jaarsveld, M.T., Hollestelle, A., Prager-van der Smissen, W.J., Heine, A.A., Boersma, A.W., Liu, J., Helmijr, J., Ozturk, B., Smid, M., et al. (2013). miRNA expression profiling of 51 human breast cancer cell lines reveals subtype and driver mutation-specific miRNAs. Breast Cancer Res. *15*, R33.

Sanchez-Garcia, F., Villagrasa, P., Matsui, J., Kotliar, D., Castro, V., Akavia, U.D., Chen, B.J., Saucedo-Cuevas, L., Rodriguez Barrueco, R., Llobet-Navas, D., et al. (2014). Integration of genomic data enables selective discovery of breast cancer drivers. Cell *159*, 1461–1475.

Shah, S.P., Roth, A., Goya, R., Oloumi, A., Ha, G., Zhao, Y., Turashvili, G., Ding, J., Tse, K., Haffari, G., et al. (2012). The clonal and mutational evolution spectrum of primary triple-negative breast cancers. Nature *486*, 395–399.

Shao, D.D., Tsherniak, A., Gopal, S., Weir, B.A., Tamayo, P., Stransky, N., Schumacher, S.E., Zack, T.I., Beroukhim, R., Garraway, L.A., et al. (2013). ATARiS: computational quantification of gene suppression phenotypes from multisample RNAi screens. Genome Res. *23*, 665–678.

Shi, J., and Vakoc, C.R. (2014). The mechanisms behind the therapeutic activity of BET bromodomain inhibition. Mol. Cell *54*, 728–736.

Solimini, N.L., Xu, Q., Mermel, C.H., Liang, A.C., Schlabach, M.R., Luo, J., Burrows, A.E., Anselmo, A.N., Bredemeyer, A.L., Li, M.Z., et al. (2012). Recurrent hemizygous deletions in cancers may optimize proliferative potential. Science *337*, 104–109.

Sørlie, T., Perou, C.M., Tibshirani, R., Aas, T., Geisler, S., Johnsen, H., Hastie, T., Eisen, M.B., van de Rijn, M., Jeffrey, S.S., et al. (2001). Gene expression patterns of breast carcinomas distinguish tumor subclasses with clinical implications. Proc. Natl. Acad. Sci. USA *98*, 10869–10874.

Stagni, V., Manni, I., Oropallo, V., Mottolese, M., Di Benedetto, A., Piaggio, G., Falcioni, R., Giaccari, D., Di Carlo, S., Sperati, F., et al. (2015). ATM kinase sustains HER2 tumorigenicity in breast cancer. Nat. Commun. *6*, 6886.

Stephens, P.J., Tarpey, P.S., Davies, H., Van Loo, P., Greenman, C., Wedge, D.C., Nik-Zainal, S., Martin, S., Varela, I., Bignell, G.R., et al.; Oslo Breast Cancer Consortium (OSBREAC) (2012). The landscape of cancer genes and mutational processes in breast cancer. Nature *486*, 400–404.

Stratikopoulos, E.E., Dendy, M., Szabolcs, M., Khaykin, A.J., Lefebvre, C., Zhou, M.M., and Parsons, R. (2015). Kinase and BET Inhibitors Together Clamp Inhibition of PI3K Signaling and Overcome Resistance to Therapy. Cancer Cell *27*, 837–851.

Takemoto, M., Fukuda, T., Sonoda, R., Murakami, F., Tanaka, H., and Yamamoto, N. (2002). Ephrin-B3-EphA4 interactions regulate the growth of specific thalamocortical axon populations in vitro. Eur. J. Neurosci. *16*, 1168–1172.

Tibes, R., Qiu, Y., Lu, Y., Hennessy, B., Andreeff, M., Mills, G.B., and Kornblau, S.M. (2006). Reverse phase protein array: validation of a novel proteomic technology and utility for analysis of primary leukemia specimens and hematopoietic stem cells. Mol. Cancer Ther. *5*, 2512–2521.

Timmerman, L.A., Holton, T., Yuneva, M., Louie, R.J., Padró, M., Daemen, A., Hu, M., Chan, D.A., Ethier, S.P., van 't Veer, L.J., et al. (2013). Glutamine sensitivity analysis identifies the xCT antiporter as a common triple-negative breast tumor therapeutic target. Cancer Cell *24*, 450–465.

Worby, C.A., and Dixon, J.E. (2014). Pten. Annu. Rev. Biochem. *83*, 641–669.

Yousif, N.G., Al-Amran, F.G., Hadi, N., Lee, J., and Adrienne, J. (2013). Expression of IL-32 modulates NF-κB and p38 MAP kinase pathways in human esophageal cancer. Cytokine *61*, 223–227.

Yu, F., Li, J., Chen, H., Fu, J., Ray, S., Huang, S., Zheng, H., and Ai, W. (2011). Kruppel-like factor 4 (KLF4) is required for maintenance of breast cancer stem cells and for cell migration and invasion. Oncogene *30*, 2161–2172.

Zender, L., Xue, W., Zuber, J., Semighini, C.P., Krasnitz, A., Ma, B., Zender, P., Kubicka, S., Luk, J.M., Schirmacher, P., et al. (2008). An oncogenomics-based in vivo RNAi screen identifies tumor suppressors in liver cancer. Cell *135*, 852–864.

Zhang, L., Zhang, Y., Mehta, A., Boufraqech, M., Davis, S., Wang, J., Tian, Z., Yu, Z., Boxer, M.B., Kiefer, J.A., et al. (2015). Dual inhibition of HDAC and EGFR signaling with CUDC-101 induces potent suppression of tumor growth and metastasis in anaplastic thyroid cancer. Oncotarget *6*, 9073–9085.